The Cumulus Parameterization Problem in the Context of MJO Simulations

Jun-Ichi Yano

CNRM, Meteo-France
42 av Coriolis
31057 Toulouse Cedex, France
E-mail: yano@cnrm.meteo.fr
&
L. M. D.
B–99, Universite Pierre-et-Marie-Curie
4, place Jussieu
75252 Paris cedex 05, France.
E-mail: yano@lmd.jussieu.fr

ABSTRACT

Issues in cumulus parameterizations in the context of global MJO simulations are discussed. In attempting to close a parameterization by convective–scale energetics, it is important to realize that CAPE (convective available potential energy) is better interpreted as a measure of energy convertibility rather than as a potential energy. A generalization of CAPE as a potential energy convertibility (PEC) is suggested. The entrainment rate that recovers the buoyancy associated with PEC by an entrainment plume model is estimated from CRM experiments for the three phases of a MJO cycle. The result suggests the entrainment is order of magnitude larger than the previously adopted values, thus the suppression of convection by dry intrusion is rectified, but it tends to remain invariant with time. Finally, an analysis of the energy cycle of a MJO simulated by a global model in wavelet space is presented as a possible method for identify the associated mechanisms.

1 Overview: Cumulus Parameterization Problem: CISK or WISHE?

The purpose of the present talk is to address some of the basic issues in the cumulus parameterizations in simulating MJO in global models, and also present a possible method for diagnosing the role of cumulus convection in global simulations of MJO. It is well accepted that MJO is a consequence of interactions between the large–scale tropical dynamics and cumulus convection. Thus, it is reasonable to expect that our ability of simulating MJO is much impaired by problems of cumulus parameterizations in global models, as it appears to be the case.

In order to set a scene, this presentation begins with a brief overview on the current status of the cumulus parameterizations from a theoretical point of view. It would not be quite an oversimplification to say that the theoretical studies of MJO last one decade have turned around the controversies between CISK and WISHE (*cf.*, Emanuel *et al.* 1994). Thus, a certain retrospective view may be useful after one decade of unsettled, rather fruitless debates.

In retrospect, in fact, these debates were not so wide divided as they appeared. These two major completing theories for MJO, both CISK and WISHE, are based on an assumption of a quasi–stationary balance of the large-scale system in moisture and energy budgets, respectively. That is the assumption that a large–scale supply of a quantity is well balanced by its consumption by deep convection at any moment, reducing to Arakawa and Schubert's quasi–equilibrium hypothesis when CAPE is taken as such a quantity, but the CISK argument is equivalent, when CAPE is replaced by moisture.

A physically–based quasi–equilibrium principle in the sense as introduced by Arakawa and Schubert (1974) is questioned by Yano *et al.* (2000) from quantitative observational analyses (see also Yano 1999, 2003a). The $1/f$-noise behavior found in convective variability (Yano *et al.* 2001b, 2003b) rather implies that the system is far away from equilibrium, a state generally called the self–criticality in statistical mechanics (*cf.*, Sornette 2000). In this opposite state, not only the statistical–mean quantities, but specific details of the individual fine–scale elements (such as cold pools in the boundary layer) critically control the subsequent evolution of the whole system (as in triggering). From these respects, a critical revision of the MJO theory appears to be necessary.

Being said this, nevertheless, I also believe that the critical examinations for determining the limits of the quasi–stationary theory, as defined above, are still to be performed. In this respect, since the WISHE theory is based on the budget of CAPE, the critical examination of the concept of CAPE warrants some scrutiny. An improvement of these conventional frameworks based on the assumption of quasi–stationary balance is proposed, and applied to CRM simulations of TOGA–COARE period in the next section. As a possible method for objectively diagnosing the role of cumulus convection in global models, the analysis of energy cycles is considered in Section 3.

2 Generalization of CAPE: Potential Energy Convertibility (PEC)

2.1 Formulation

CAPE is defined as a work W performed by buoyancy b of a hypothetically–lifted air parcel:

$$d\text{CAPE} = dW = b\, dz. \tag{2.1}$$

Thus, it describes a process that converts the potential energy into the kinetic energy by a work. In other words, CAPE is a measure of convertibility of energy, rather than a measure of potential energy itself.

This point is more clearly seen by taking a time derivative on Eq. (2.1), which leads to

$$\frac{dW}{dt} = b\frac{dz}{dt} = b\, w. \tag{2.2}$$

Here, the vertical velocity w is introduced by $w \equiv dz/dt$. A vertical integral of Eq. (2.2) provides a rate of generation of kinetic energy for a given atmospheric column:

$$\int_0^H \rho \frac{dW}{dt} dz = \int_0^H \rho w b\, dz. \tag{2.3}$$

Here, the density ρ is multiplied on the integrand so that the energy generation rate per column (*i.e.*, [W/m^2]) is obtained after integral. We take the integral over the whole troposphere (from the surface $z = 0$ to the tropopause level, H). A standard definition of CAPE is recovered by setting $\rho w = 1$ in Eq. (2.3).

Conversely, we can generalize the concept of CAPE as a rate of conversion of energy (Eq. 2.3) normalized by a measure of the vertical momentum $(\rho w)^*$:

$$PEC = \int_0^H b^*\, dz, \tag{2.4}$$

which we call the potential energy convertibility (PEC). Here, we have introduced an effective buoyancy b^* by

$$b^* \equiv \frac{\rho w}{(\rho w)^*} b. \tag{2.5}$$

The measure of vertical momentum $(\rho w)^*$ is here, defined by a root–square–mean over the atmospheric column, *i.e.*, $(\rho w)^* \equiv \{\overline{\int_0^H (\rho w)^2\, dz/H}\}^{1/2}$. The horizontal–domain mean is also applied on $(\rho w)^*$, as designated by $\overline{\ }$, in order to facilitate a separation of the rate of generating kinetic energy into the parts due to the buoyancy forcing (*i.e.*, PEC) and those due to the vertical motions (*i.e.*, $(\rho w)^*$) in terms of the domain–mean budget, as in the following analyses.

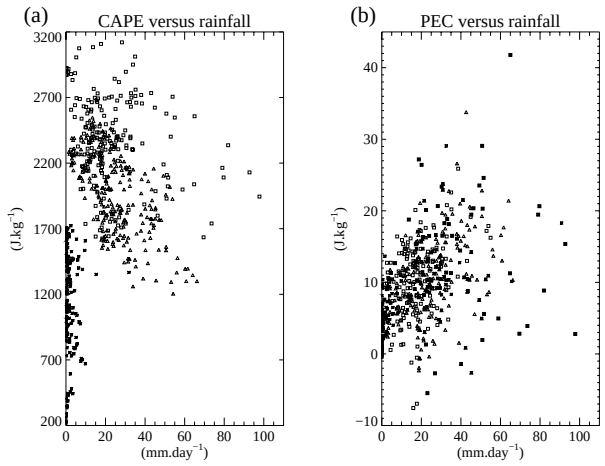

Figure 1: Scatter plots (a) between the precipitation and CAPE, (b) between the precipitation and PEC, based on data averaged every 30 min.

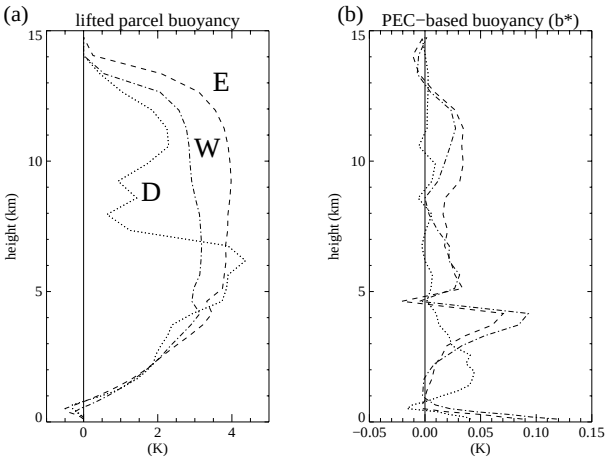

Figure 2: Mean vertical profiles of (a) parcel–lifted (CAPE) buoyancy, and (b) convection–driving (PEC) buoyancy. Cases D, E, W are shown by dotted, long–dash, dotted–dash lines.

2.2 CRM analysis results

The above formulation is applied to the three CRM simulations of TOGA–COARE period, corresponding to the different phases of MJO. Those correspond to a dry intrusion event (14–18 November 1992: asterisk $*$, case D), a easterly–wind regimes (10–14 December 1992: square, case E) and a westerly–wind burst (20–24 December 1992: triangle $\triangle$, case W).

For the analyses, both b and w locally prognosed in CRM are used. Thus, the effective buoyancy b^* (2.5) gives the *convection–driving* buoyancy in a domain–mean sense. The results are summarized in Fig. 1 in terms of the scatter plots (a) between CAPE and rainfall, as well as (b) between PEC and rainfall. The different simulations are marked by different symbols as indicated above. We see that CAPE recovers to a value higher than 1000 J/kg even an aftermath of the dry intrusion event, although it strongly suppressed convective rainfall for an extended period. Thus, CAPE does not work as an instantaneous measure of deep convective variability. In comparison, PEC varies more linearly with rainfall, indicating that this can be used as a better diagnostic measure for convection.

The mean parcel–lifted buoyancy b_p and PEC-based buoyancy b^* profiles are shown in Fig. 2 (a) and (b), respectively, for these CRM experiments. The standard parcel–lifted buoyancy provides almost identical profile up to a 6 km level, although above that level the buoyancy for the dry–intrusion period is substantially

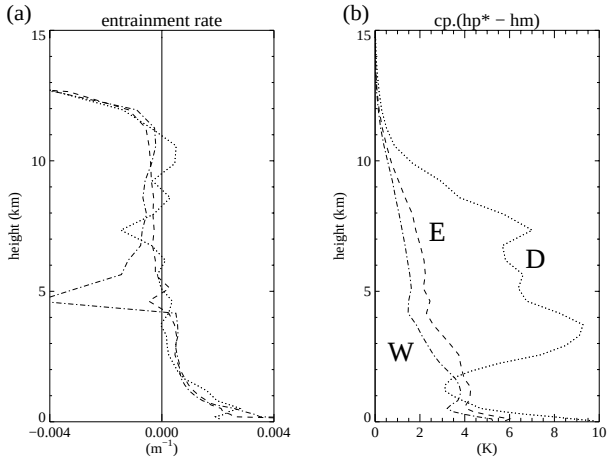

Figure 3: Mean vertical profiles of (a) the entrainment rate estimated from convection–driving buoyancy, and (b) the dryness of environment, $h_p^* - h_e$, in unit of temperature K .

suppressed. On the other hand, the PEC–based convection–driving buoyancy is consistently smaller for the dry–intrusion case for all the vertical levels, except for a narrow zone of 1–3 km height. In this manner, the PEC–based diagnosis more directly depicts how the system is dynamically driven by buoyancy in a domain–mean sense.

2.3 Estimate of entrainment rates

The CRM analysis of the previous subsection shows that the PEC–based convection–driving buoyancy, defined by Eq. (2.5), provides a better measure of convective instability than the standard parcel–lifted buoyancy, b_p. Thus, the performance of CAPE–based cumulus parameterizations would be improved, if the scheme could predict the buoyancy profile as diagnosed for PEC. Recall that many of the parameterizations use entrainment plume models. For these parameterizations, this goal is achieved by adjusting the entrainment rate of environmental air into the convective updrafts.

A simple estimate of such an entrainment can be performed by assuming that the moist static energy is conserved with uplifting of a saturated air parcel, so that the entrainment rate λ is estimated from the equation

$$\frac{\partial}{\partial z} h_p^* = -\lambda (h_p^* - h_e), \tag{2.6}$$

where h_p^* is the saturated lifted–parcel moist–static energy, estimated from the PEC-buoyancy b^*, h_e is the environmental (domain–mean) moist static energy. In estimating h_p^* from b^*, we first evaluate the virtual temperature of the air parcel from the PEC-based buoyancy b^*, then estimate the parcel temperature assuming the saturation of the air parcel. The obtained temperature is directly used to compute the saturated moist static energy h_p^*.

The obtained estimates of the entrainment rates are shown in Fig. 3 (a), along with the vertical profile of $h_p^* - h_e$ (in the unit of temperature dividing it by C_p) in Fig. 3 (b).

Interestingly, the estimated entrainment rate is relatively unchanged over the three phases of MJO. Thus, the time–mean of the estimated entrainment could be used in parameterizations. Nevertheless, convection is substantially suppressed after the dry intrusion, because the dryness of the environment, as measured by $h_p^* - h_e$, controls the entrainment effect. During this period, the system is convectively less unstable as a result. It appears that in this manner, the dryness of the free troposphere controls the convective variability over the MJO cycle, as already speculated by various authors (*e.g.*, Grabowski 2003, Grabowski and Moncrieff 2003). Here, we have provided more direct quantitative evidence for this moisture–convective feedback.

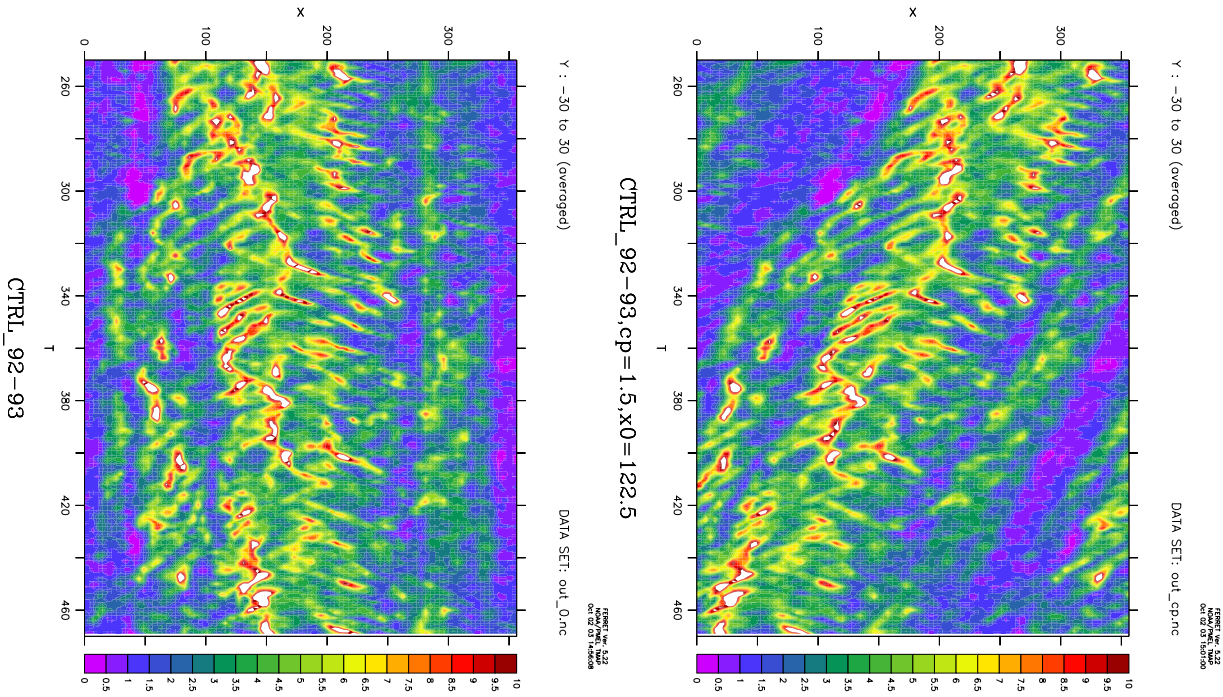

Figure 4: Time–longitude section of precipitation over $30^\circ S$–$30^\circ N$ *as simulated by LMDZ (left). The same as the left, but after a Galilean transform with the phase velocity of* $c_p = 1.5$ *m/s (right).*

The estimated entrainment rate ($\sim 10^{-3}$) is an order of magnitude larger than the value typically used for deep convective parameterizations ($\sim 10^{-4}$: *e.g.*, Tiedtke 1989). This may explain a relative insensitivity of current schemes on dry intrusions and thus, their failure to simulate MJO.

3 Global Energetics of MJO

3.1 Formulation

Fig. 4 shows an example of simulations by the LMDZ global climate model as a longitude–time section of the tropical total precipitation (averaged over 30°S and 30°N). Here, interestingly enough, something looks like MJO that are propagating eastwards are indeed simulated, although the propagation speed is obviously few times too slow (c_p = 1.5 m/s). Thus, it is possible to diagnose the degree of success and failures of the modelling by analyzing such features.

We specifically take the energetics as such an analysis tool by asking how energetically these features are maintained. Here, we essentially take the global energy cycle proposed by Lorenz (1955), as typically called the Lorenz's four boxes (*e.g.*, Peixóto and Oort 1974; Oort and Peixóto 1992, Ch. 13, 14). Such an energy cycle analyses has already been applied to MJO by Yanai *et al.* (2000). These energetics are summarized in the Appendix B.

However, the main problem of applying this approach to MJO under the conventional frameworks of zonal–eddy interactions or under further decompositions into the wavenumber modes is that it does not capture features associated with MJO, which are localized in space. In order to overcome this problem, we perform the energy cycle analysis in the wavelet space, in which we identify MJO by a single wavelet mode,[1] and examine the energy budget concerning this MJO–wavelet mode.

[1] Or more generally, by a selected set of modes. This aspect would be important for full analysis considering the variables whose peaks are shifted longitudinally. This is, however, neglected in this preliminary report.

For this purpose, all the physical variables are expanded by wavelets in the longitudinal direction (λ), *e.g.*,

$$\mathbf{v}(\lambda,\varphi,p,t) = \sum_l \tilde{\mathbf{v}}_l(\varphi,p,t)\psi_l(\lambda) \tag{3.1a}$$

$$\alpha'(\lambda,\varphi,p,t) = \sum_l \tilde{\alpha}_l(\varphi,p,t)\psi_l(\lambda) \tag{3.1b}$$

for the horizontal velocity components $\mathbf{v}$ and the specific volume α. The prime for the latter designates the deviation from the average, $\overline{\alpha}$, at constant pressure surface over the analysis domain (30°S–30°N). Here, the wavelets ψ_l are characterized by an index l (see Yano *et al.* 2001a, 2003), and $\tilde{\mathbf{v}}_l$ and $\tilde{\alpha}_l$ are the expansion coefficients, which depend on latitude φ, pressure height p, and time t. These arguments are omitted for simplicity in the following. Here, we use the Meyer wavelet.

We analyze in the wavelet space, the budget of the kinetic energy and the (available) potential energy defined by

$$\tilde{K}_l = \tilde{\mathbf{v}}_l^2/2, \tag{3.2a}$$

$$\tilde{P}_l = \tilde{\alpha}_l^2/2\overline{S}, \tag{3.2b}$$

respectively, where

$$S = -\frac{\alpha}{\theta}\frac{\partial\theta}{\partial p} \tag{3.3}$$

is a measure of the stratification (with θ the potential temperature), and its average over the horizontal analysis domain (represented by overbar $\overline{\ }$) is used in the definition of the potential energy.

The standard energy integral in the wavelet space defines the energy cycle of the system by

$$\frac{\partial\tilde{K}_l}{\partial t} + \tilde{B}_l^K + \tilde{N}_l^K = \tilde{C}_l - \tilde{D}_l, \tag{3.4a}$$

$$\frac{\partial\tilde{P}_l}{\partial t} + \tilde{B}_l^P + \tilde{N}_l^P = -\tilde{C}_l + \tilde{G}_l. \tag{3.4b}$$

Under this energy cycle, the potential energy is generated by the rate

$$\tilde{G}_l = (\frac{R}{pC_p\overline{S}})\tilde{\alpha}_l\tilde{Q}_l + \frac{C_v}{pC_p}\sum_{n,m} < \psi_l\psi_n\psi_m > \tilde{\omega}_n\tilde{P}_{lm} - \frac{\tilde{\alpha}_l}{\overline{S}}\frac{\partial\overline{\alpha}}{\partial t} - \frac{\tilde{\alpha}_l^2}{2\overline{S}^2}\frac{\partial\overline{S}}{\partial t} \tag{3.5a}$$

and converted into the kinetic energy with the rate

$$\tilde{C}_l = -\tilde{\omega}_l\tilde{\alpha}_l. \tag{3.5b}$$

The kinetic energy is dissipated with the rate

$$\tilde{D}_l = -\tilde{\mathbf{v}}_l\cdot\tilde{\mathbf{F}}_l. \tag{3.5c}$$

Thus, the potential energy is primarily generated by a positive correlation of buoyancy (which is proportional to α') and the diabatic heating rate Q. The last three terms in Eq. (3.4a) represent minor contributions due to the gradual change of the reference state. The potential energy is converted into the kinetic energy, when a positive correlation exists between buoyancy α' and the vertical velocity $-\omega$. This term is the large–scale counterpart of PEC, introduced in Section 3, which measures the analogous process in convective scales.. Finally, the kinetic energy is dissipated by dissipative forcing $\mathbf{F}$ as given by Eq. (3.5c). Here, R and C_p are the gas constant and the heat capacity at constant pressure, respectively; $C_v = C_p - R$; $< * >$ designates an average over longitude; $\tilde{P}_{lm}$ is defined by Eq. (A.2b) in Appendix A.

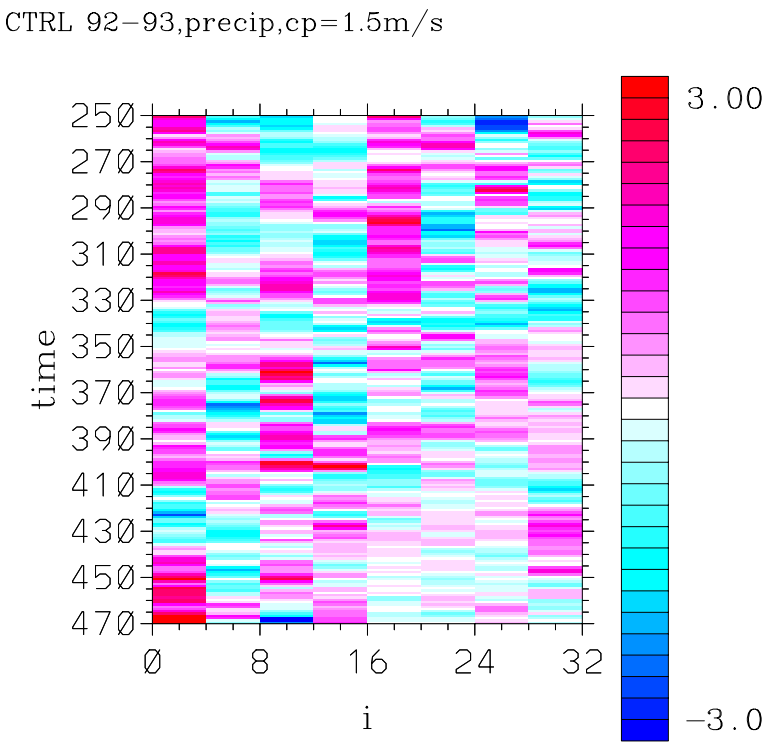

Figure 5: The wavelet transform of the right frame of Fig. 4: the spatial localization (horizontal axis) of the "wavenumber" 8 precipitation field as the function of time (vertical axis).

Furthermore, the energy is exchanged through lateral boundaries (NB: a latitudinal band of 30°S–30°N is used for the analysis domain below) by $\tilde{B}_l$ and transformed from different wavelet–modes by $\tilde{N}_l$. Both are more precisely defined by sums of triad modes:

$$\tilde{B}_l = \sum_{n,m} < \psi_l \psi_m \psi_n > \tilde{B}_{lnm}, \tag{3.6a}$$

$$\tilde{N}_l = \sum_{n,m} \tilde{N}_{lnm}. \tag{3.6b}$$

The expressions for the specific terms $\tilde{B}_{lnm}$ and $\tilde{N}_{lnm}$ are involved and given in the Appendix A, separately.

3.2 Results

For the analysis purpose, the system is first Galilean transformed on the coordinate moving with the propagation speed ($c_p = 1.5$ m/s eastwards) of MJO–like features, as shown in the right frame of Fig. 4. Then, the wavelet transform is applied in the longitudinal direction, as defined by Eq. (4.1). We adopt the Meyer wavelet as in our previous studies. The obtained wavelet coefficient for the "wavenumber" 8, a dominant scale for these MJO–like features, is shown in Fig. 5 with the spatial localization (index i) and the time as the horizontal and the vertical axes, respectively. The two MJO–like events seen in the real space are identified as the 5th and the 3rd modes from the left in this wavelet spectrum. We identify them as MJO modes in our analysis.

The energy budget for this identified 1st MJO mode (5th wavelet mode with the "wavenumber" 8) is summarized in Fig. 6. As expected for the tropics, the available potential energy (APE, long–dash, a) is much smaller than the kinetic energy (solid, a) for the whole period considered. Rather surprisingly, generation of APE by diabatic heating G (solid, b) is very small, and most of APE for this MJO mode is supplied by nonlinear energy transfer, N^P (chain–dash, b). Almost exactly the same amount of APE is converted into the kinetic energy (the term C, long–dash in b, and solid in c) at any moment, a kind of quasi–stationary balance, but quite different

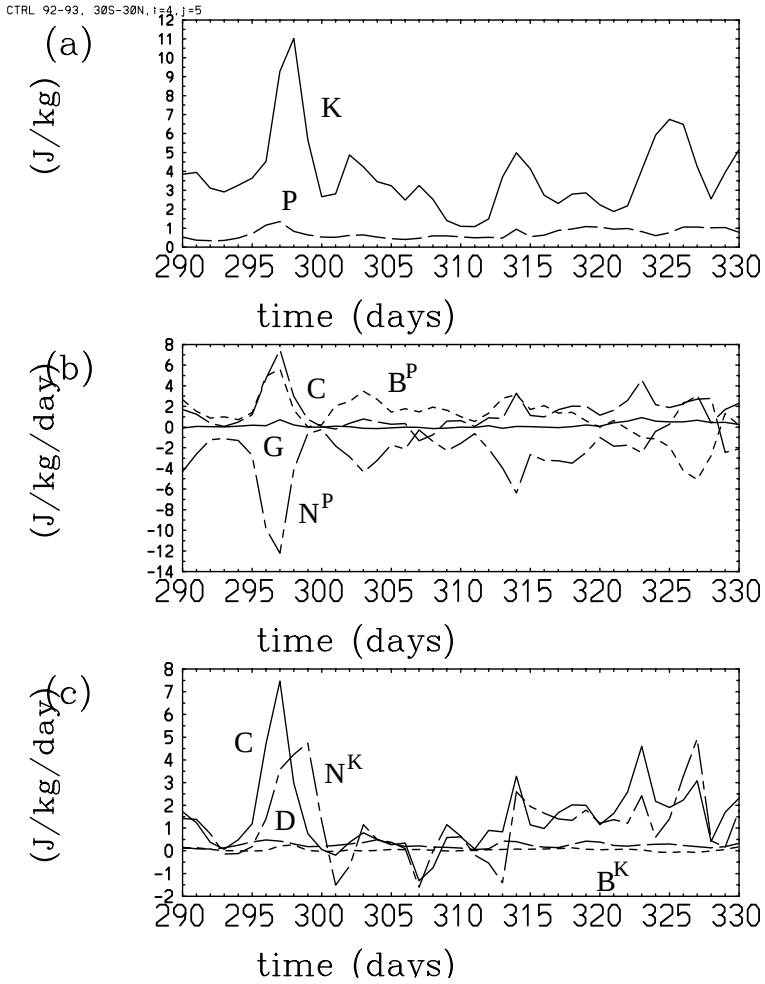

Figure 6: The energy budget of the wavelet MJO mode as functions of time. (a) The kinetic energy (solid), and the potential energy (long–dash). (b) The energy budget for the potential energy: the energy generation rate G (solid), the conversion rate C (long–dash), the lateral forcing B^P (short–dash), and the nonlinear transfer N^P (chain–dash). (b) The energy budget for the kinetic energy: the energy conversion rate C (solid), the dissipation rate D (long–dash), the lateral forcing B^P (short–dash), and the nonlinear transfer N^P (chain–dash).

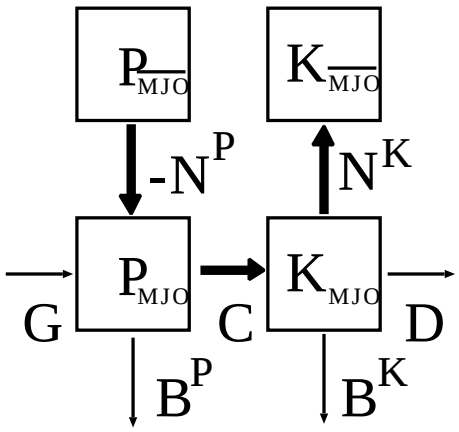

Figure 7: The schematics of the energy cycle identified for MJO in LMDZ simulation. The potential energy for the MJO mode is primarily generated by nonlinear interactinos, which are converted into the kinetic energy, which is lost by nonlinear interactions in turn.

from what the convective quasi–equilibrium theory predicts (*i.e.*, a close balance between G and C). The generated kinetic energy is lost by nonlinear energy transfer (term N^K, chain–dash in c) at the almost same rate, in turn. Dissipation term, D (long–dash in c) is small, against what the linear theories predict, in which this term must balance with the energy conversion C.

The energy cycle of MJO diagnosed from the LMDZ simulation is summarized in Fig. 7. The most important aspect is that this MJO is, dynamically, not at all forced by convection, but rather forced by nonlinear transfer of potential energy from larger scales. This is a great deal of contrast with the current standard theories as well as what implied by a global data analysis by Yanai *et al.* (2000, compare their Fig. 10 and 11).

4 Summary

• Objective quantification of moisture–convection feedback is provided and applied to the MJO dynamics. For this purpose, the potential energy convertibility (PEC) is proposed as a generalization of CAPE, which provides more realistic estimate of convection–driving buoyancy for convective parameterizations. The estimated entrainment required for an entraining plume model in order to recover the PEC–based buoyancy profile is an order of magnitude larger than the one used in current parameterizations. Thus, the realistic parameters predict much more sensitivity of deep convection on tropospheric moisture, which appears to control the MJO cycle.

• In order to understand the mechanism for MJO–like features in GCM, the energy cycle is diagnosed in the wavelet space. In a LMDZ simulation, the potential energy for MJO is generated by nonlinear transfer, presumably associated with deformation of strong latitudinal temperature gradients, which is in turn converted into the kinetic energy. A lack of generation of potential energy by convective heating, as assumed in majority of current theories, may indicate a major defect of this model.

• At the workshop, the results obtained at ECMWF during my visit for 20–24 November 2003 will also be presented.

acknowledgements

The present work has been performed in collaborations with Jean-Pierre Chaboureau, Francoise Guichard, Jean-Yves Grandpeix, Ionela Musat, Peter Bechtold, Adrian Tompkins. The visit to ECMWF during 20–24

November 2003 was made possible by arrangements by Anton Beljaars. Pascal Marquet has carefully verified the derivation in Appendix B.

5 References

Arakawa, A., and W. H. Schubert, 1974: Interaction of a cumulus cloud ensemble with the large–scale environment, part I, *J. Atmos. Sci.*, **31**, 674–701.

Emanuel, K. A., J. D. Neelin, and C. S. Bretherton, 1994: On large–scale circulations in convecting atmosphere. *Quart. J. Roy. Meteor. Soc.*, **120**, 1111–1143.

Grabowski W. W., 2003: MJO–like coherent structures: Sensitivity simulations using the cloud–resolving convection parameterization (CRCP). *J. Atmos. Sci.*, **60**, 847–864.

Grabowski W. W., and M. W. Moncrieff, 2003: Moisture–convective feedback in the tropics. submitted to *Quart. J. Roy. Meteor. Soc.*

Lorenz, E. N. (1955). Available potential energy and the maintenance of the general circulation. *Tellus*, **7**, 157–167.

Peixóto, J. P., and A. H. Oort (1974). The annual distribution of atmospheric energy on a planetary scale. *J. Geophys. Res.*, **79**, 2149–2159.

Peixoto, J. P. and A. H. Oort (1992). *Physics of climate*. American Institute of Physics, New York, 520pp.

Sornette, D., 2000: *Critical Phenomena in Natural Sciences : Chaos, Fractals, Selforganization and Disorder : Concepts and Tools*. (Springer Series in Synergetics, 450 pp.

Tiedtke, M., 1989: A comprehensive mass flux scheme of cumulus parameterization in large–scale models. *Mon. Wea. Rev.*, **117**, 1779–1800.

Yanai, M., B. Chen, W.-W. Tung, 2000: The Madden–Julian oscillation observed during the TOGA COARE IOP: Global view. *J. Atmos. Sci.*, **57**, 2374–2396.

Yano, J.-I., 1999: Scale–separation and quasi-equilibrium principles in Arakawa and Schubert's cumulus parameterization. *J. Atmos. Sci.*, **56**, 3821–3823.

Yano, J.-I., 2003: Comments on "Remarks on quasi–equilibrium theory" by D. K. Adams and N. O. Rennó. *J. Atmos. Sci.*, **60**, 2342–2343. <http://www.aero.obs-mip.fr/chajp/yanji/ar.ps>

Yano, J.-I., W. W. Grabowski, G. L. Roff, and B. E. Mapes, 2000 : Asymptotic approaches to convective quasi–equilibrium. *Quart. J. Roy. Meteor. Soc.*, **126**, 1861–1887.

Yano, J.-I. M. W. Moncrieff, X. Wu, and M. Yamada, 2001a : Wavelet analysis of simulated tropical convective cloud systems Part I: Basic analysis. *J. Atmos. Sci.*, **58**, 850-867. <http://www.aero.obs-mip.fr/chajp/yanji/wavelet1.ps>

Yano, J.-I., K. Fraedrich, and R. Blender, 2001b: Tropical convective variability as $1/f$–noise. *J. Climate*, **14**, 3608–3616. <http://www.aero.obs-mip.fr/chajp/yanji/noise.ps>

Yano, J.-I. , P. Bechtold, J.-L. Redelsperger, and F. Guichard, 2003a: Wavelet–Compressed Representation of deep moist convection. submitted to *Mon. Wea. Rev.*
<ftp://ftp.lmd.jussieu.fr/pub/yano/compress/ms.pdf>
<ftp://ftp.lmd.jussieu.fr/pub/yano/compress/fig_list.pdf>

Yano, J.-I. , R. .Blender, Chidon Zhang, and K. Fraedrich, 2003b: $1/f$–Noise and Pulse–like Events in the Tropical Atmospheric Surface Variabilities. submitted to *Quart. J. Roy. Meteor. Soc.*
<ftp://ftp.lmd.jussieu.fr/pub/yano/pulse>

Appendix A: Energy balance: Nonlinear terms

Individual triads for lateral forcing in Eq. (3.6a) are given by

$$\tilde{B}^K_{lnm} = \mathscr{D}_\lambda(\tilde{K}_{lm}\tilde{\mathbf{v}}^3_n) + \mathscr{D}_\lambda(\tilde{\Phi}_l\tilde{\mathbf{v}}^3_l)\delta_{ln}\delta_{nm}, \tag{A.1a}$$

$$\tilde{B}^P_{lnm} = \mathscr{D}_\lambda(\tilde{P}_{lm}\tilde{\mathbf{v}}^3_n), \tag{A.1b}$$

where

$$\tilde{K}_{lm} = \tilde{\mathbf{v}}_l \cdot \tilde{\mathbf{v}}_m, \tag{A.2a}$$

$$\tilde{P}_{lm} = \tilde{\alpha}_l\tilde{\alpha}_m/\overline{S}, \tag{A.2b}$$

the operator $\mathscr{D}_\lambda$ is defined by

$$\mathscr{D}_\lambda(\mathbf{A}) = \frac{1}{a\cos\varphi}(\frac{\partial}{\partial\varphi}\cos\varphi A_\varphi)_p + \frac{\partial}{\partial p}A_p, \tag{A.2c}$$

and $\mathbf{v}^3_l = (\tilde{\mathbf{v}}_l, \omega_l)$ is the three–dimensional velocity.

The two expressions are possible for the triads terms for nonlinear energy transfer in Eq. (3.6b). When the advection form is used, one obtains

$$\tilde{N}^K_{lnm} = \frac{1}{a\cos\varphi} < \psi_l\psi_n\frac{\partial\psi_m}{\partial\lambda} > \tilde{u}_n\tilde{K}_{lm} - < \psi_l\psi_n\psi_m > [\frac{\tilde{\mathbf{v}}_m}{a\cos\varphi}\cdot\frac{\partial}{\partial\varphi}\tilde{v}_n\tilde{\mathbf{v}}_l\cos\varphi + \tilde{\mathbf{v}}_m\cdot\frac{\partial}{\partial p}\tilde{\omega}_n\tilde{\mathbf{v}}_l]$$
$$+\frac{\delta_{nm}}{a\cos\varphi} < \psi_l\frac{\partial\psi_n}{\partial\lambda} > (\tilde{u}_l\tilde{\Phi}_n + \tilde{u}_n\tilde{\Phi}_l) \tag{A.3a}$$

$$\tilde{N}^P_{lnm} = \frac{1}{a\cos\varphi} < \psi_l\psi_n\frac{\partial\psi_m}{\partial\lambda} > \tilde{u}_n\tilde{P}_{lm} - \frac{< \psi_l\psi_n\psi_m >}{\overline{S}}[\frac{\tilde{\alpha}_m}{a\cos\varphi}\frac{\partial}{\partial\varphi}\tilde{v}_n\tilde{\alpha}_l\cos\varphi + \tilde{\alpha}_m\frac{\partial}{\partial p}\tilde{\omega}_n\tilde{\alpha}_l]$$
$$+\frac{< \psi_l\psi_n\psi_m >}{\overline{S}}\tilde{P}_{lm}\tilde{\omega}_n\frac{\partial\overline{S}}{\partial p} \tag{A.3b}$$

When the flux form is used, one obtains

$$\tilde{N}^K_{lnm} = -\frac{1}{a\cos\varphi} < \frac{\partial\psi_l}{\partial\lambda}\psi_n\psi_m > \tilde{u}_n\tilde{K}_{lm} - < \psi_l\psi_n\psi_m > [\tilde{v}_n(\frac{\tilde{\mathbf{v}}_m}{a}\cdot\frac{\partial}{\partial\varphi}\tilde{\mathbf{v}}_l) + \tilde{\omega}_n(\tilde{\mathbf{v}}_m\cdot\frac{\partial}{\partial p}\tilde{\mathbf{v}}_l)]$$
$$+\frac{\delta_{nm}}{a\cos\varphi} < \psi_l\frac{\partial\psi_n}{\partial\lambda} > (\tilde{u}_l\tilde{\Phi}_n + \tilde{u}_n\tilde{\Phi}_l) \tag{A.4a}$$

$$\tilde{N}^P_{lnm} = -\frac{1}{a\cos\varphi} < \frac{\partial\psi_l}{\partial\lambda}\psi_n\psi_m > \tilde{u}_n\tilde{P}_{lm} - \frac{< \psi_l\psi_n\psi_m >}{\overline{S}}\tilde{\alpha}_m(\frac{\tilde{v}_n}{a}\frac{\partial}{\partial\varphi} + \tilde{\omega}_n\frac{\partial}{\partial p})\tilde{\alpha}_l$$
$$+\frac{< \psi_l\psi_n\psi_m >}{\overline{S}}\tilde{P}_{lm}\tilde{\omega}_n\frac{\partial\overline{S}}{\partial p} \tag{A.4b}$$

Appendix B: Standard Energetics

We consider the energetics of the primitive equation system with the pressure coordinate, in which the momentum and the thermodynamic equations are, respectively, given by

$$\frac{D}{Dt}\mathbf{v} + f\mathbf{k}\times\mathbf{v} = -\nabla\Phi + \mathbf{F}, \tag{B.1}$$

$$(\frac{\partial}{\partial t} + \mathbf{v}\cdot\nabla)T + \frac{T}{\theta}\frac{\partial\theta}{\partial p}\omega = \frac{Q}{C_p}. \tag{B.2}$$

Here, notations are standard with most of the variables defined in the main text. In performing the energy integrals, we write the thermodynamic equation (B.2) in terms of the specific volume α by using the relationship $\alpha = RT/p$. We obtain,

$$(\frac{\partial}{\partial t} + \mathbf{v}\cdot\nabla)\alpha + \frac{\alpha}{\theta}\frac{\partial\theta}{\partial p}\omega = \frac{RQ}{pC_p}. \tag{B.3}$$

The energy integral is performed by multiplying $\mathbf{v}$ and α on Eq. (B.1) and (B.3), respectively. Here, we keep the differential forms instead of actually performing the integrals.

After some manipulations (with a help of mass continuity, notably), we obtain the conservation laws for the kinetic energy

$$K = \frac{\mathbf{v}^2}{2}, \tag{B.4a}$$

and the (available) potential energy

$$P = \frac{\alpha'^2}{2\overline{S}}, \tag{B.4b}$$

respectively, which are given by

$$\frac{\partial}{\partial t}K + \nabla\cdot\mathbf{v}K + \frac{\partial}{\partial p}\omega K = F + C - D \tag{B.5a}$$

$$\frac{\partial}{\partial t}P + \nabla\cdot\mathbf{v}P + \frac{\partial}{\partial p}\omega P = -C + G \tag{B.5b}$$

with

$$G = \alpha'\frac{RQ}{pC_p\overline{S}} - (\frac{C_v}{pC_p})\frac{\alpha'^2\omega}{\overline{S}} - \frac{\alpha'}{\overline{S}}(\frac{\partial\overline{\alpha}}{\partial t}) - \frac{\alpha'^2}{2\overline{S}^2}(\frac{\partial}{\partial t} + \omega\frac{\partial}{\partial p})\overline{S} \tag{B.6a}$$

$$C = -\alpha'\omega \tag{B.6b}$$

$$F = -[\nabla\cdot\mathbf{v}\Phi' + \frac{\partial}{\partial p}\omega\Phi'] \tag{B.6c}$$

$$D - \mathbf{v}\cdot\mathbf{F} \tag{B.6d}$$

Here, $\Phi' = \Phi - \overline{\Phi}$ is the perturbation geopotential defined as a deviation from a reference profile $\overline{\Phi}(p,t)$, which only depends on height p, and possibly on time t. The perturbation specific volume $\alpha' = \alpha - \overline{\alpha}$ is also defined similarly. Note that the two variables are connected by the hydrostatic balance:

$$\frac{\partial\Phi'}{\partial p} = -\alpha'. \tag{B.6}$$

The last two terms of Eq. (B.5b) vanishes when a time–independent reference state is used. The energy conversion terms (B.6) are defined analogously as in the wavelet space in the main text. Especially, the third term from the last in Eq. (B.6a) is another unphysical term arising from a need for defining a reference state in this formulation.

Appendix C: Analysis Procedures

As many other global models, LMDZ uses a hybrid vertical coordinate, which combines features of p– and σ–coordinates. For the analysis purpose, we consider it as a generalized vertical coordinate defined by $\xi = \xi(x,y,p)$. Conversely, the pressure level for a given vertical level ξ (which is further reinterpreted as a level index after discretizations) is $p = p(x,y,\xi)$. Note that the formulation for the energetics in the main text is given in terms of the p–coordinate system. Thus, few special cares are required in order to apply this formulation to a system with a more general vertical coordinate. Our strategy is to perform the analysis at the pressure levels $p(x,y,\xi)$ of the model, but by reinterpreting it in terms of the p–coordinate system.

Most importantly, the vertical velocity, ω_ξ, of LMDZ is given by the rate of mass exchange over a constant ξ–surface (more precisely, over a interface of model layers), $p(x,y,\xi)$, but translating it into the unit of pressure change. The ω–velocity in p–coordinate system can be recovered by the relation

$$\omega = \omega_\xi + (\frac{\partial}{\partial t} + \mathbf{v}\cdot\nabla)_\xi p(x,y,\xi), \tag{C.1}$$

where the subscript ξ implies the operations are performed by retaining ξ constant. As a minor technicality, the horizontal velocity $\mathbf{v}$ defined at middle layer levels is linearly interpolated onto the pressure interfaces. After this conversion, the advection terms can be treated as in the p–coordinate system.

In defining the reference state for α, we have computed α at the mean pressure, $\bar{p}(\xi)$, for a given ξ–level under a linear approximation:

$$\alpha(\bar{p}(\xi)) \simeq \alpha(\bar{p}(x,y,\xi)) - \frac{\partial\alpha(\bar{p}(x,y,\xi)}{\partial p}\delta p(x,y,\xi), \tag{C.2}$$

where $\delta p(x,y,\xi) = p(x,y,\xi) - \bar{p}(\xi)$ is the deviation of the pressure level from the mean.

The wavelet transform is performed at constant ξ–levels, assuming the deviation from a constant pressure surface is small. The validity of this assumption is checked by comparing the reference state $\bar{\alpha}$ evaluated with and without above corrections (C.2).

Finally, the pressure gradient term is evaluated by

$$\nabla_p\Phi' = \nabla_\xi\Phi' + \alpha'\nabla_\xi p. \tag{C.3}$$

This relation is obtained with a help of the hydrostatic balance (B.6). Notably,

$$< \psi_l\frac{\partial\psi_n}{\partial\lambda} >_p \tilde{\Psi}_n = < \psi_l\frac{\partial\psi_n}{\partial\lambda} >_\xi \tilde{\Psi}_n + \tilde{\alpha}_n\sum_m < \psi_l\psi_n\frac{\partial\psi_m}{\partial\lambda} >_\xi \tilde{p}_m. \tag{C.4}$$